energies

MDPI

Article

Dimensioning Air Reactor and Fuel Reactor of a Pressurized CLC Plant to Be Coupled to a Gas Turbine: Part 2, the Fuel Reactor

Wang Lu [1], Pietro Bartocci [2,*], Alberto Abad [2], Aldo Bischi [3], Haiping Yang [1], Arturo Cabello [2], Margarita de Las Obras Loscertales [2], Mauro Zampilli [4] and Francesco Fantozzi [4]

[1] State Key Laboratory of Coal Combustion, Huazhong University of Science and Technology, Wuhan 430074, China; luwang721@hust.edu.cn (W.L.); yhping2002@163.com (H.Y.)
[2] Instituto de Carboquímica (C.S.I.C.), C. Miguel Luesma Castán 4, 50018 Zaragoza, Spain; abad@icb.csic.es (A.A.); acabello@icb.csic.es (A.C.); mobras@icb.csic.es (M.d.L.O.L.)
[3] Department of Energy, Systems, Territory and Construction Engineering, University of Pisa, Largo Lucio Lazzarino 1, 56122 Pisa, Italy; aldo.bischi@unipi.it
[4] Department of Industrial Engineering, University of Perugia, Via G. Duranti 67, 06125 Perugia, Italy; mauro.zampilli@unipg.it (M.Z.); francesco.fantozzi@unipg.it (F.F.)
* Correspondence: pbartocci@icb.csic.es

Abstract: Bioenergy with Carbon Capture and Storage (BECCS) technologies are fundamental to reach negative CO_2 emissions by removing it from the atmosphere and storing it underground. A promising solution to implement BECCS is pressurized Chemical Looping Combustion (CLC), which involves coupling a pressurized CLC reactor system to a turboexpander. The typical configuration chosen is to have an air reactor and a fuel reactor based on coupled circulating fluidized beds. The fluidization regime in both reactors is preferred to be fast fluidization to enhance gas particle contact and solids circulation among reactors. To design the two reactors, Aspen Plus software was used, given that the new version has a module for fluidized bed modeling. At first, the oxygen carrier was designed ex novo, but given that it is a composite compound mainly made by nickel oxide freeze-granulated on alumina (Ni40Al-FG), the molecular structure has been inserted in Aspen Plus. Then, based on the power of the gas turbine, the power output per kg of evolving fluid (in this case, depleted air) is calculated using Aspen Plus. Once the nitrogen content in the depleted air is known, the total air at the inlet of the air reactor is calculated. The fuel reactor is modeled by inserting the reduction reactions for nickel-based oxygen carriers. The paper presents a useful methodology for developing pressurized Chemical Looping Combustors to be coupled to gas turbines for power generation. The provided data will be cross-validated with 0D-models and experimental results.

Keywords: carbon negative technologies; gas turbines; pressurized chemical looping combustor; biofuels; BECCS

Citation: Lu, W.; Bartocci, P.; Abad, A.; Bischi, A.; Yang, H.; Cabello, A.; de Las Obras Loscertales, M.; Zampilli, M.; Fantozzi, F. Dimensioning Air Reactor and Fuel Reactor of a Pressurized CLC Plant to Be Coupled to a Gas Turbine: Part 2, the Fuel Reactor. *Energies* **2023**, *16*, 3850. https://doi.org/10.3390/en16093850

Academic Editors: Roberta De Robbio and Maria Cristina Cameretti

Received: 3 August 2022
Revised: 7 November 2022
Accepted: 18 April 2023
Published: 30 April 2023
Corrected: 23 July 2024

1. Introduction

According to Kang et al. [1], more than 120 nations have made carbon neutrality pledges at current times [2,3]. In this context, Carbon Capture and Storage (CCS) is considered an irreplaceable technology to achieve this target [4]. Together with CCS, the development of Negative Emissions Technologies (NET) is also advocated [5]. These are key technologies that are able to absorb CO_2 directly from the atmosphere and store it underground, while CCS is used "only" to prevent CO_2 from reaching the atmosphere and increasing the carbon dioxide concentration. Examples of NET are afforestation and reforestation, the increase of carbon content in soils, storing carbon in the soils in the form of biochar, Bioenergy with Carbon Capture and Storage (for BECCS see also [6]), Direct Air Carbon Capture and Storage (DACCS), and enhanced weathering and ocean fertilization [7]. However, what is the Technology Readiness Level of the many NET? In an

interesting report from the Royal Society and Royal Academy of Engineering, the TRL of NETs is displayed in Table 1 [8].

Table 1. TRL of most important NETs [8].

NET Technology	TRL
Afforestation, reforestation, and forest management [9–11]	8–9
Wetland, peatland, and coastal habitat restoration [10]	5–6
Soil carbon sequestration [9,12]	8–9
Biochar [9,12,13]	3–6
Bioenergy with carbon capture and storage [11,14]	Bioenergy: 7–9 CCS: 4–7
Ocean fertilization [15,16]	1–5
Building with biomass [17]	8–9
Enhanced terrestrial weathering [11]	1–5
Mineral carbonation [18]	3–8
Ocean alkalinity [19,20]	2–4
Direct air capture [12,21,22]	4–7
Low-carbon concrete [18,23,24]	6–7

It can be seen in Table 1 that the TRL of Bioenergy with Carbon Capture and Storage (BECCS) technologies depend on the TRL of bioenergy production technologies. These are needed to produce biofuel (which can be solid, gaseous, and liquid), and the TRL of Carbon Capture and Storage technologies (which are needed to capture and store carbon dioxide). While bioenergy technologies have a high technology readiness level, carbon capture technologies have a lower TRL level, which is comparable to that of direct air capture. On the other hand, there is no agreement in the literature on the TRL of BECCS because this is a category of technologies that have different TRLs [25]. For example, from the data reported by Möllersten [25], we can infer that 2G bioethanol with carbon capture can be considered TRL 5–6, while biomethane with carbon capture can be considered TRL 7–8; 1G bioethanol with CCS has a TRL ranging from 7 to 9; biomass power with CCS has a TRL of 7–8. For what has been said above, the question "What is the TRL of BECCS?" implies another question, which is: "What is the TRL of CCS?" An interesting classification of CCS technologies is proposed in Table 2 [26].

Table 2. Classification of Carbon Capture and Storage based on their TRL [26].

TRL	Technology
high technology readiness level—TRL (7–9)	1. Chemical Absorption 2. Physical Absorption 3. Membrane Permeation 4. Pre-combustion 5. Cryogenic distillation
low technology readiness level—TRL (≦7)	1. Hybrid coupling among cryogenic distillation, membrane permeation, and chemical or physical absorption 2. Enhanced chemical or physical absorption 3. Gas-liquid membrane contractors 4. Adsorption 5. Oxy-combustion 6. Chemical Looping Combustion 7. Mineralization

This paper is particularly focused on the Chemical Looping Combustion (CLC) process. In the work of Di Giuliano et al. [27], it is stated that the TRL of CLC is probably about 6, this is in agreement with what reported also in the report of the Global CCS Institute "Technology Readiness and costs of CCS" [28]. Chemical Looping Combustion is a technology in which combustion oxygen is provided by a metal oxide (named oxygen carrier), which is reduced while the fuel is oxidized. This happens in a reactor named FUEL

REACTOR (see Figure 1). Then, the oxygen carrier is regenerated in the AIR REACTOR (see Figure 1) oxidizing with air and the reduced metal. Oxidation and the reduction of the metal happen separately in two different reactor grants and, from the air reactor, a flow of depleted air is generated (mainly containing less oxygen than the incoming air due to the fact that some oxygen is consumed by oxidation). Additionally, a flow of carbon dioxide and water vapor is obtained from the fuel reactor. By condensing water vapor, a pure flow of carbon dioxide is obtained, which can be compressed and stored.

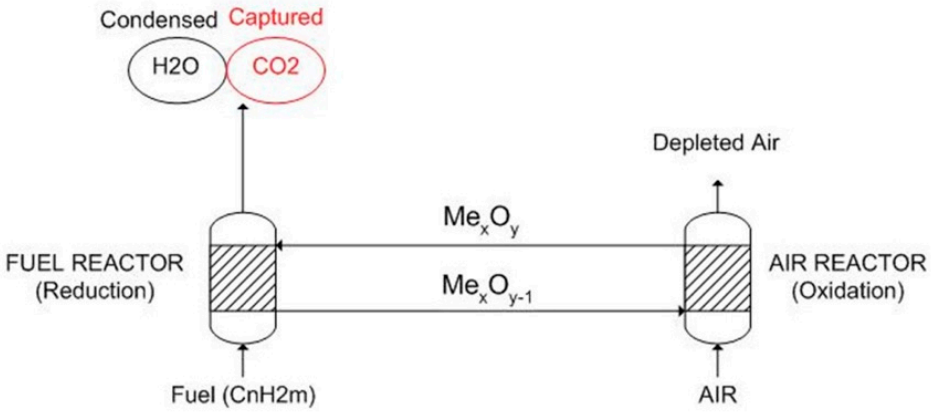

Figure 1. The Chemical Looping Combustion process [29].

The advantages of Chemical Looping Combustion are represented by the fact that when technological feasibility is proved and when plants will be scaled up the cost of carbon capture with this technology will be probably the lowest on the market and also the energy penalty linked with it. To develop Bioenergy with Carbon Capture and Storage (BECCS) technology based on Chemical Looping Combustion, two main routes can be followed: one is to produce steam that can be expanded into a steam turbine and the other is to couple the chemical looping combustor with a gas turbine. The latter configuration is supposed to achieve higher efficiency of the final power generation plant. On the other hand, when coupling a chemical looping combustor with a gas turbine, pressurizing both the chemical reactor and the air reactor is needed. This represents a technological barrier, which is addressed in the Marie Curie project: GTCLC-NEG. In this project, the following configuration of plant is proposed (see Figure 2).

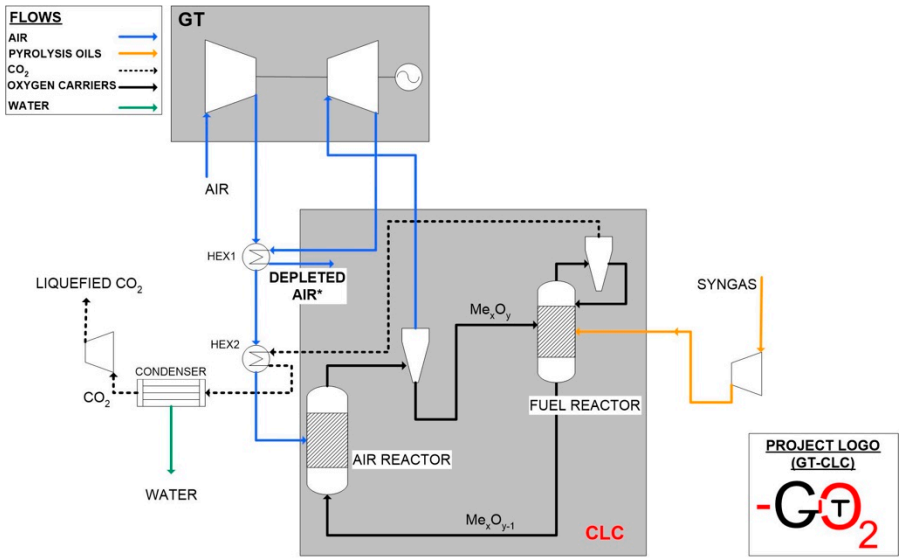

Figure 2. The GTCLC-NEG concept [29].

We can see in Figure 2 that air is at first compressed to about 12 bars and then enters the air reactor, which is a fluidized bed working at fast fluidization regime. Then, depleted air passes through a cyclone and expands in the gas turbine. The process is similar to what happens also in externally fired gas turbines. The expanded air has still a relevant temperature, so the waste heat is recovered in the first heat exchanger (HEX1). The cooled air is released to the environment. The fuel reactor can be fed with different biofuels (such as syngas or biogas or even solid biofuels, such as wood chips). These have to also be pressurized in a compressor at 12 bars. When the biofuels react with the oxygen carriers, they are converted to carbon dioxide and water vapor. After passing through a cyclone, the exhaust gases produced at the fuel reactor are also heated up to a temperature at about 1200 °C. Usually, the oxidation reaction is exothermic, while the reduction reaction can be either endothermic or exothermic. The waste heat in this case is recovered by the second heat exchanger (HEX2) which is also used to separate the water vapor from the CO_2 by condensing the water vapor. We obtain in this way a pressurized flow of carbon dioxide that can be further compressed to liquify it and then transported to the storage location.

To optimize the efficiency of the plant, an ASPEN Plus model has been realized in this paper we present the results of the design phase of the fuel reactor, while in [29], the results of the design phase of the air reactor is presented. We leave out of the analysis the cyclone, which is an important component and needs to be analyzed.

2. Materials and Methods

2.1. Methodology Followed to Design the Fuel Reactor

The methodology followed for the design of the fuel reactor is similar to that used for the air reactor, presented in [29] and adapted from [30,31]; see Figure 3. We see in Figure 3 that the design process is divided into two parts:

- The part that uses fuel characteristics, oxygen carrier characteristics, and oxidation and reduction reactions kinetics to calculate mass balances, reactor inventory, and solids circulation rate. This part first takes into account the air reactor because it is the one which is directly connected to the gas turbine and then the fuel reactor mass flows are determined based on stoichiometric calculations referred to the fuel needed to reduce the oxidized oxygen carrier. The dimensions of the reactor are set considering the optimal velocity of fluidization and the entrainment of particles;
- In the second part, the dimensions of the reactor and the optimal velocities are double checked using the Grace diagram to calculate the fluidization regime and checking that this is close to the fast fluidization regime.

The fuel reactor has one more criticality respect to the air rector: the chemical reactions happening significantly change the properties of the gases inside the reactor. In fact, in the case of the air reactor depleted air has quite similar properties respect the air fed into the reactor at the inlet. On the other hand, the density, viscosity, and velocities of the fuel are completely different from those of the reduction products, such as: carbon dioxide and water vapor. For this reason, the introduction of chemical reactions in the fuel reactor is of key importance and so it is the use of reactions kinetics derived at pressurized conditions. Simulation of reactions in fluidized bed is not new in Aspen Plus. Research have focused mainly on biomass gasification [32–35] and coal combustion in circulating fluidized beds [36]. The advantage of chemical looping combustion respect to biomass gasification in the specific case examined in this paper is that we use already syngas composed by mainly hydrogen and carbon monoxide and so the reactions which happen in the reactor result to be simpler. The reactions and the reaction kinetic constants are introduced directly in the "Fluidbed" model which makes the simulation also easier to perform.

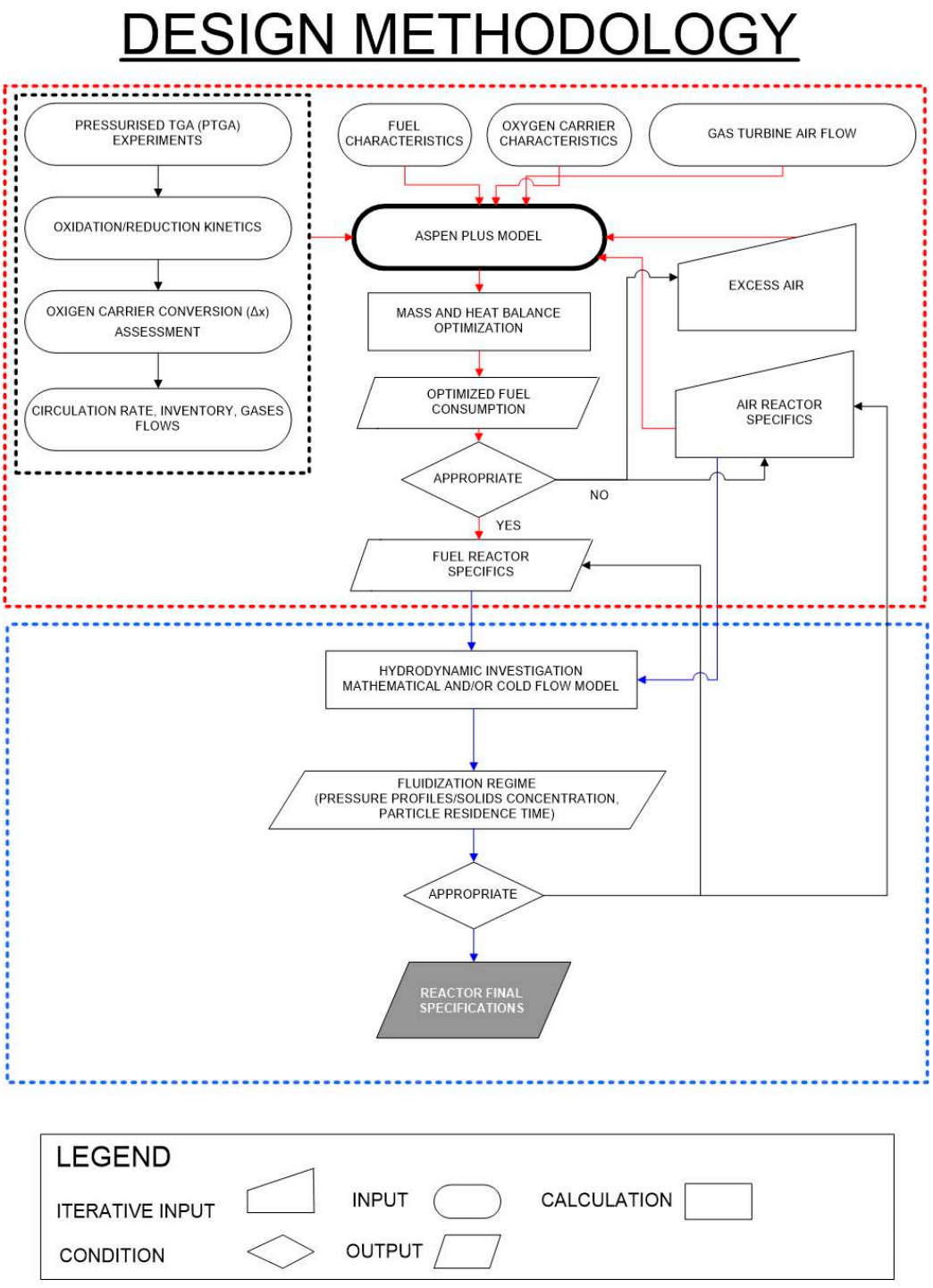

Figure 3. Methodology used to design the fuel reactor [29].

2.2. Oxygen Carrier Main Characteristics

The main characteristics of the oxygen carrier used are shown in Table 3. The oxygen carrier is derived from a freeze granulation (FG) preparation process, performed at Chalmers University, according to what was reported in [37], and it contains 40% of nickel oxide in weight. It is identified accordingly with the abbreviation Ni40Al-FG.

Table 3. Ni40Al-FG Oxygen carrier characteristics [38].

Parameter	Value	Unit of Measure
Active NiO content	40	wt%
Oxygen transport capacity, R_0	0.084	-
Particle size	0.2	μm
Porosity	0.36	%
Specific surface area (BET)	0.8	m^2/g
Solid density	5380	kg/m^3

On the Aspen Plus software components section, when selecting an oxygen carrier to be inserted as a component the ID should be introduced in form of the chemical formula of the compound (e.g., Al_2O_3-NiO); if this identity is not recognized as a compound contained in the database linked with Aspen Plus software, the compound has to be user defined, specifying the following parameters:

- Component ID and Alias are identified as the compound chemical formula;
- Compound state (in the case of the oxygen carrier we consider solid state);
- Molecular weight;
- Normal boiling point;
- Solid enthalpy of formation;
- Solid Gibbs energy of formation;
- Molar volume data (here also the density of the solid can be inserted);
- Vapor pressure data;
- Extended Antoine vapor pressure coefficients;
- Solid heat capacity data;
- Solid heat capacity polynomial coefficient.

The final data, after they have been inserted in the software, are proposed in Table 4. Dealing with the solid heat capacity coefficient, the solid molar volume, these are estimated based on the polynomial of alumina (Al_2O_3) and Nickel (Ni and NiO), which are assumed to be inserted separately, given that it is assumed that there is no chemical interaction between the two. Another step is represented by the necessity to model the Particle Size Distribution (PSD) inside the air reactor a PSD mesh is used, and it can be seen in Table 4, as calculated with Apen Plus V11. To realize the mesh a distribution function is built. This is based on the GGS (Gates–Gaudin–Schuhmann) approach; see [39]. The dispersion parameter is set to 1.5 and the maximum diameter is set to 0.4 mm. The minimum value of the distribution is set to 0.1 mm.

Table 4. Kinetic analysis of the oxygen carrier reduction [38].

Interval	Lower Limit	Upper Limit (μm)	Weight Fraction (μm)	Cumulative Weight Fraction
1	100	130	0.185279	0.185279
2	130	160	0.0677037	0.252982
3	160	190	0.0743889	0.327371
4	190	220	0.0805198	0.407891
5	220	250	0.086215	0.494106
6	250	280	0.0915561	0.585662
7	280	310	0.0966021	0.682264
8	310	340	0.101397	0.783661
9	340	370	0.105975	0.889637
10	370	400	0.110363	1

The image of the PSD distribution is shown in Figure 4.

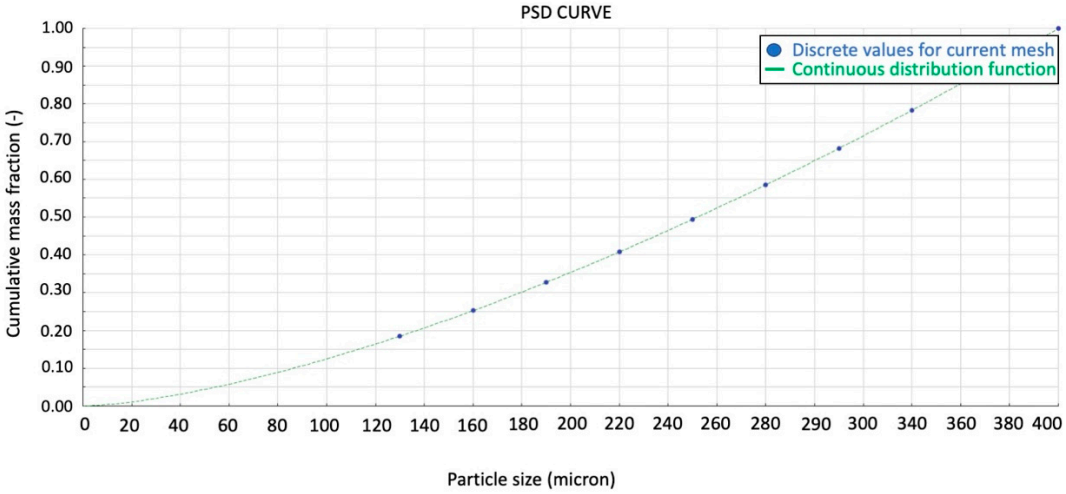

Figure 4. PSD distribution of Ni particles.

2.3. Inventory and Circulation Rate Calculations

Dealing with the circulation rate, this is defined as the mass flow of oxygen carrier which is completely oxidized [40]. This is influenced by:

- Type of oxygen carrier;
- Conversion variation obtained in the oxygen carrier;
- Type of fuel;
- Fuel reactor characteristics.

The process followed is already explained in [29], and the final value of 111 kg/s is obtained.

On the other hand, the inventory of the fuel reactor is different from that of the air reactor, even though they are both calculated in the same way as conducted in [29]. The entire process is explained in Figure 5.

As it can be seen in Figure 5, the inventory is calculated based on three main parameters:

- Characteristic circulation rate;
- Time for complete solid conversion in the reduction reaction;
- Characteristic reactivity of the FUEL REACTOR.

The time for complete solid conversion in the reduction reaction is influenced by the type of metal that is used as an oxygen carrier. This can have kinetics, which follows two main models: the plate-like geometry or the spherical grain geometry. To calculate the time for completed solid conversion in the reduction reaction, it is required that the parameter: average concentration of reacting gas in the reactor, which is calculating integrating the gas conversion rates. The parameter ε_g is the coefficient of expansion of the gas mixture and it is equal to 2 in the case of methane, 0 for hydrogen and carbon monoxide, and -0.21 in the case of oxidation. The final inventory calculated in this way is about 8000 kg of oxygen carrier. This is less than the inventory required for the air reactor and indicated in [29]. If we consider the value of inventory reported for the fuel reactor in [38] this is about 34 kg/MW with syngas composed of 45 vol% CO, 30 vol% H_2, 10 vol% CO_2, and 15 vol% H_2O and operating at a pressure of 20 bar and at a temperature of 1223 K, also assuming that water gas shift occurs. This value is referred to the power of the fuel fed into the reactor so to convert it in total kilograms we need to know the efficiency of the plant, assuming a 30% efficiency we obtain a total inventory for the fuel reactor of 1360 kg. This is reasonable when compared to our value because in [29], we have already noted that the calculated value is a theoretical one which, in practice, has to be multiplied for a safety factor that ranges between 2 and 10 times.

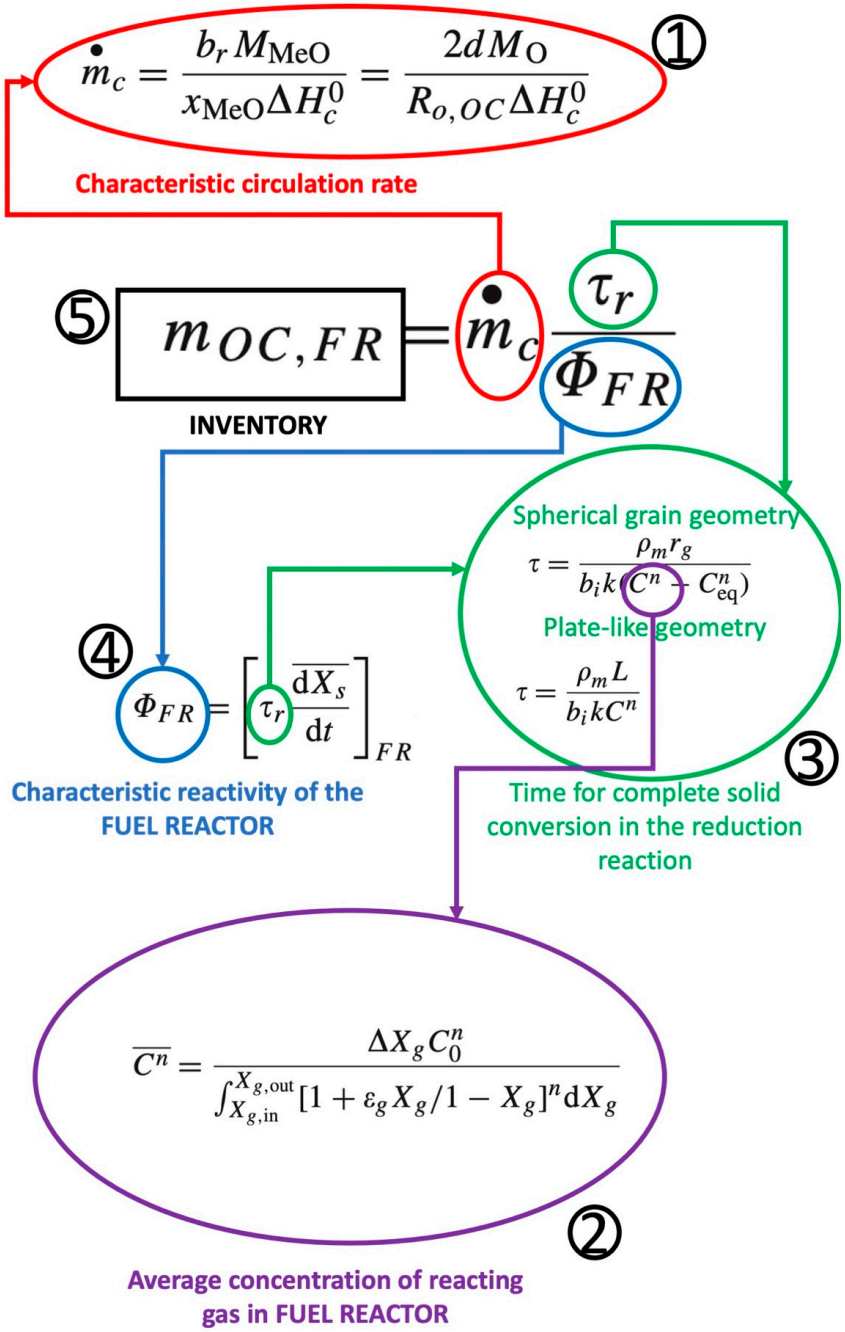

Figure 5. Method used to calculate the inventory.

2.4. Oxygen Carrier Reduction and Oxidation Reactions

From the point of view of the reactions, Equations (1) and (2) indicate reduction of carbon monoxide and hydrogen respectively (assuming that syngas is used as a fuel). Reaction 3 indicates oxidation.

$$NiO + CO \rightarrow Ni + CO_2 \quad (1)$$

$$NiO + H_2 \rightarrow Ni + H_2O \quad (2)$$

$$2Ni + O_2 \rightarrow 2\,NiO_2 \quad (3)$$

When nickel, as in this case, is used, water gas shift reaction has to also be taken into account. The kinetic of the reduction reactions is proposed in [38] and it is reported in Table 5. Where Equation (4) is the following:

$$k_{0,p} = k_0(P/P_0)^q \quad (4)$$

where $k_{0,p}$ is the preexponential factor of the chemical reaction rate constant at pressurized conditions ($mol^{1-n}\ m^{3n-2}\ s^{-1}$).

Table 5. PSD inside the fuel reactor calculated with ASPEN Plus V11.

	Symbol	H_2	CO
Molar density of metal oxide in the solid (mol MeO m^{-3} solid)	ρ_m	89,290	89,290
Stoichiometric factor in the reduction reaction of metal oxide (moles of MeO per mole of fuel gas)	b	1	1
Preexponential factor of the chemical reaction rate constant ($mol^{1-n}\ m^{3n-2}\ s^{-1}$)	k_0	9.3×10^{-3}	5.2×10^{-3}
Activation Energy ($J\ mol^{-1}$)	E	26	25
Reaction order	n	0.5	0.8
Exponent in Equation (4)	q	−0.47	−0.93
dXr/dt at 0.1 MPa	-	0.040	0.028
dXr/dt at 2.0 MPa	-	0.044	0.019

The two reduction reactions using hydrogen and carbon monoxide as fuels have been inserted in the Aspen Plus model, first defining the stoichiometry and then the kinetics; see Table 5.

3. Results

3.1. Final Design of the Fuel Reactor

The final design of the fuel reactor has been modeled with Aspen Plus, V11. As already said, this version of the software already has a model to implement a fluidized bed which is available in the section "solids" with the reactor "Fluidbed". The input parameters used to model the fuel reactor fluidized beds are reported in Table 6. Dealing with the fuel reactor the dimensions are the following: diameter: 3.0 m; height: 8 m. As can be seen in Table 7, the inventory and the circulation rate are the values that have been calculated with the help of the procedure explained in [29] and in Figure 5.

Table 6. Fluidized bed model input parameters.

Parameter	Value	Unit of Measure
Voidage at minimum fluidization	0.5	-
Geldart classification	B	-
Minimum fluidization velocity calculation method	Ergun [41]	-
Transport disengagement Height Model	George and Grace [42]	-
Maximum dCv/dh	1×10^{-5}	-
Elutriation model	Tasirin and Geldart [43]	-
Decay constant	3	-
TG parameter A1	23.7	-
TG parameter A2	14.5	-
TG parameter B1	2.5	-
TG parameter B2	2.5	-
TG parameter C1	−5.4	-
TG parameter C2	−5.4	-
Constant diameter	-	-
Cross section	circular	-
Solids discharge location	95% of total height	-
Gas distribution	injectors	-
Distributor pressure drop	0.04	bar

3.2. Profiles of Velocity, Solids Volume Fraction

In this paragraph, we present the final profiles of superficial velocity (m/s); interstitial velocity (m/s); solids volume fraction (−); and pressure (bar). The velocities inside the fuel reactor are proposed in Figure 6.

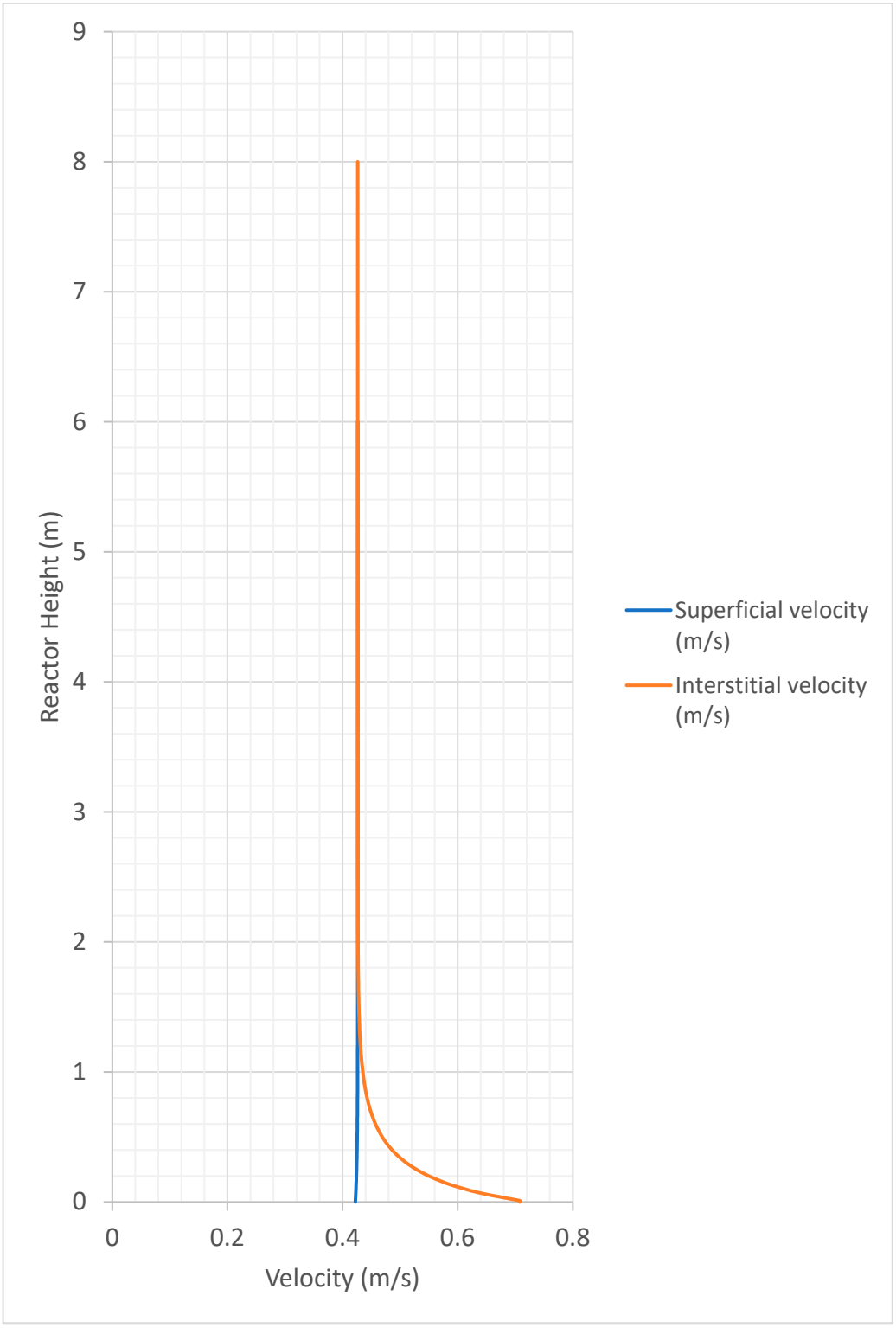

Figure 6. Velocity profiles inside the fuel reactor.

As can be seen in Figure 6, the bed of the fuel reactor is concentrated in the first 1 m of the height of the reactor. This can be seen from the interstitial velocity, which is initially higher than the superficial velocity and decreases rapidly when the freeboard begins. The final velocity value of the fuel reactor is about 0.4 m/s. The solids volume fraction in the fuel reactor is presented in Figure 7.

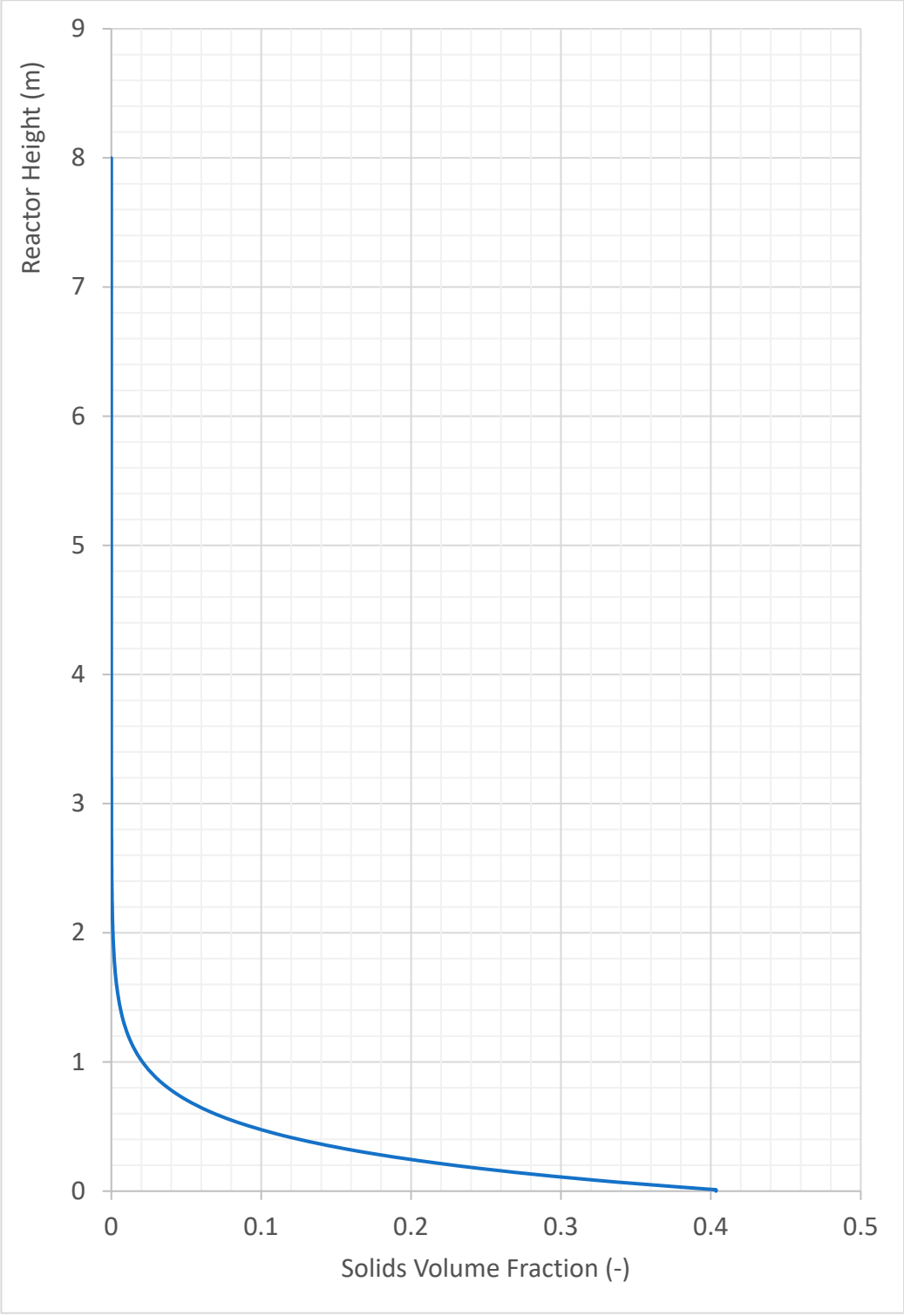

Figure 7. Solids volume fraction in the fuel reactor.

In the fuel reactor for the above-said reasons, there is less entrainment than in the air reactor.

Figure 8 confirms the data mainly reported in Table 7. The fuel reactor has high pressure in the bed zone and the pressure decreases steeply when we enter the freeboard zone.

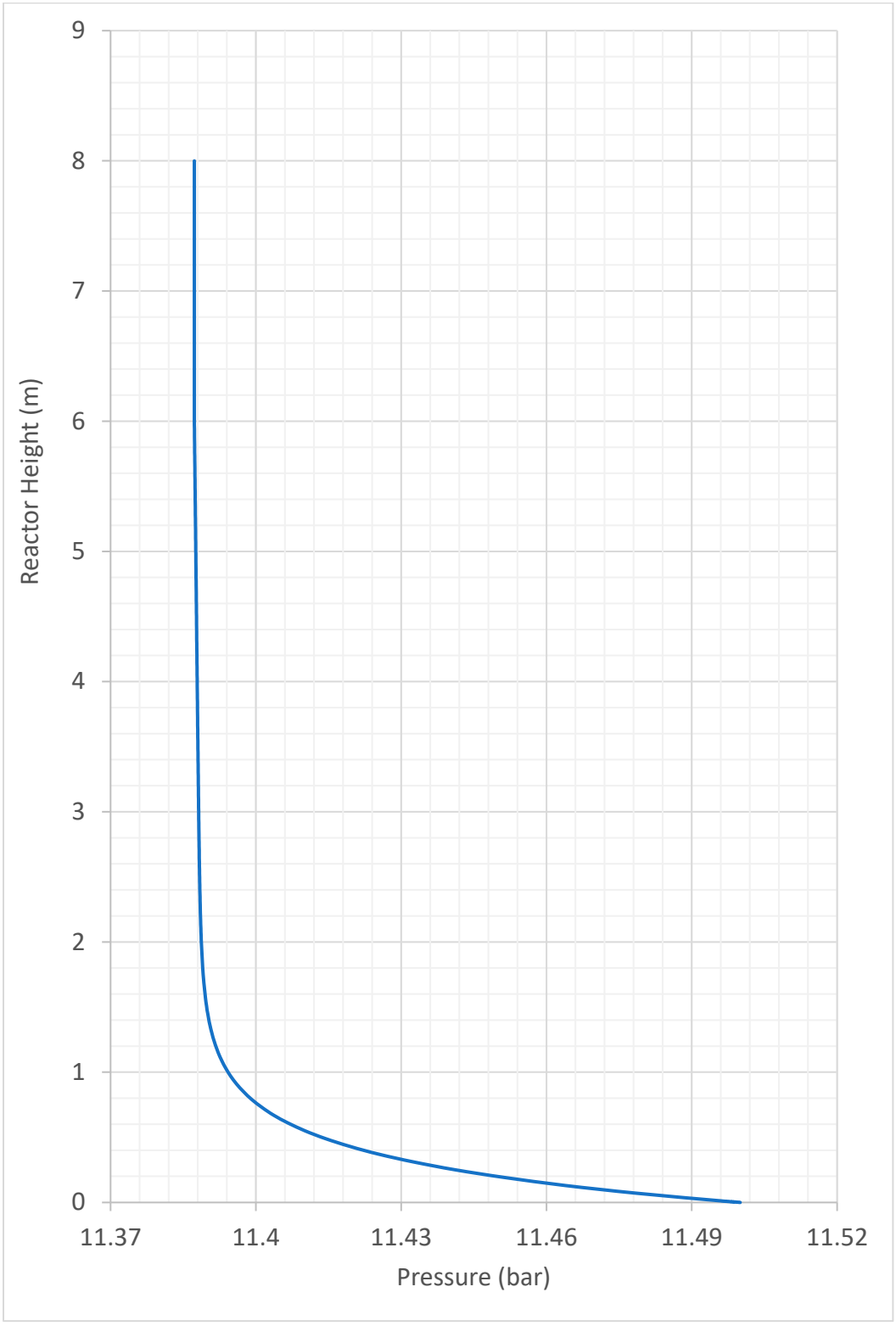

Figure 8. Pressure trend in the fuel reactor.

The decrease in the initial pressure at the inlet of the two reactors obviously represents a pressure loss, which can also have a penalty on the whole plat energy efficiency.

3.3. Profiles of Gases Concentrations

Figure 9 shows the details of the gaseous streams inside the whole fuel reactor.

It is interesting to note that the mass fractions of the gases appear to have a nonlinear trend at the height of 1 m, which is more or less when the bed transitions to the freeboard area. Depending on the position of the bubbles and of the solids, the model tries to simulate some oscillation on gas concentrations.

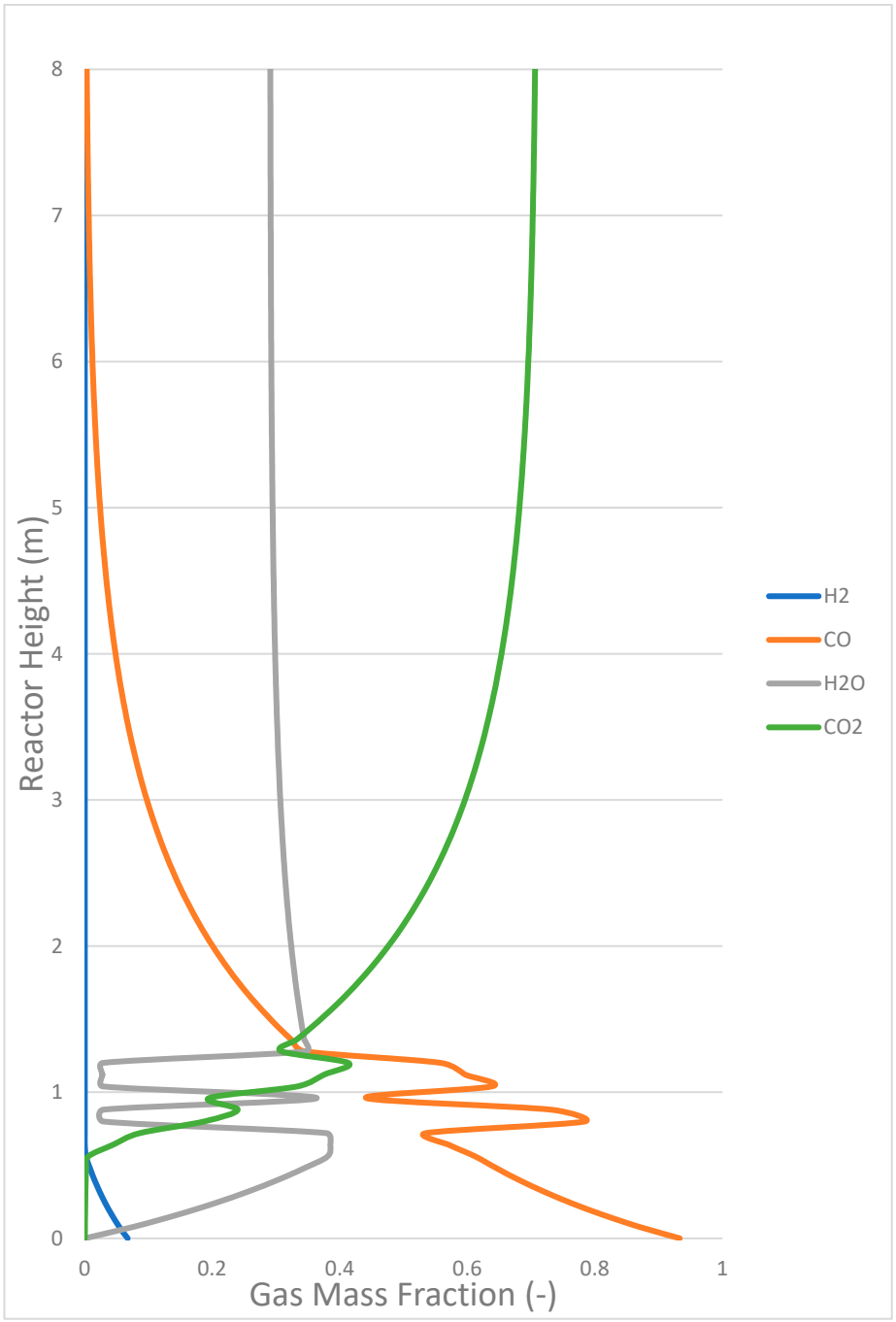

Figure 9. Gases concentrated inside the fuel reactor.

Table 7. Reactor characteristics are derived from the ASPEN Plus V11 model (Bedford, Massachusetts, U.S).

Parameter	Fuel Reactor	Unit of Measure
Total reactor height	8	m
Reactor diameter	3.0	m
Inventory	8000	kg
Circulation rate	111	kg/s
Operating pressure	12	bar
Height of bottom zone	0.01	m
Height of freeboard	5.99	m
Transport Disengaging Height calculated by correlation	5.33	m
Transport Disengaging Height based on solids volume fraction profile	3.89	m
Number of particles in bed	3.3×10^{10}	-
Surface area	26,040	sqm
Minimum fluidization velocity	0.04	m/s

3.4. Grace Diagram in the Fuel Reactor

The final calculation of the Grace diagram parameters for the fuel reactor is proposed in Figure 10.

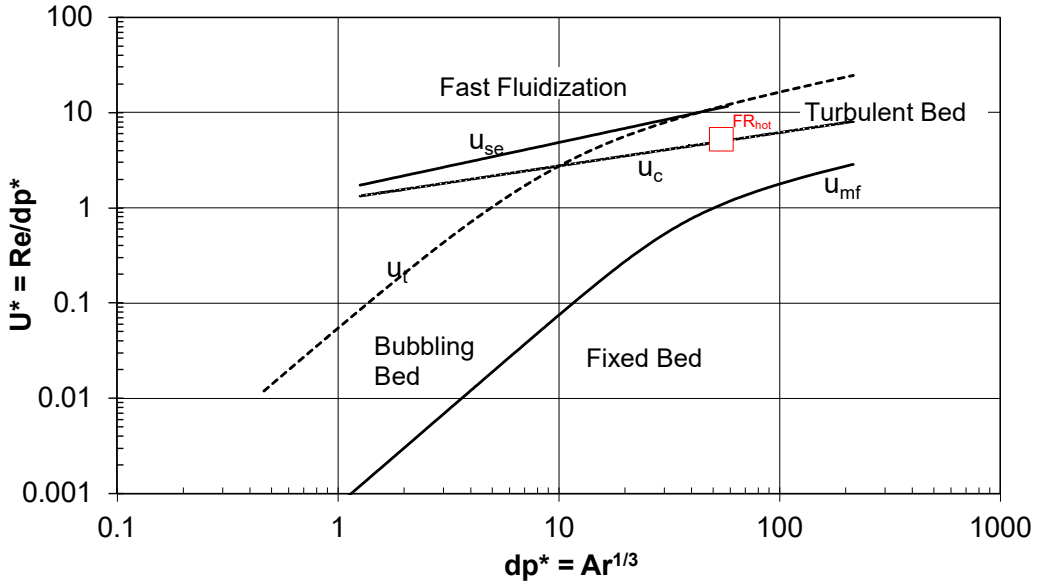

Figure 10. Grace diagram in the fuel reactor.

The two parameters described in the graph are given by the following equations, according to what is presented in [29]:

$$u^* = Re/dp^* \quad (5)$$

$$dp^* = Ar^{1/3} \quad (6)$$

$$Ar = d_p{}^3 \rho_g \, (\rho_p - \rho_g) g/\upsilon p \quad (7)$$

4. Conclusions

In this paper, the second part of the methodology, which can be used to design a Chemical Looping Combustor to be coupled to a gas turbine, is presented. In the first part, the air mass flow was calculated based on the final gas turbine power capacity; then, based on this data, the final air reactor geometry was optimized, also taking into account the oxygen carrier kinetics parameters (which influenced the circulation rate and the inventory of the air reactor). After having calculated the air needed in the air reactor and having

assumed an excess air first tentative value of 3, the stoichiometric mass flow of fuel was calculated. Based on this, the geometry of the fuel reactor was determined. Finally, the Grace diagram is used to determine the fluidization regime. The innovative aspect of this paper is the introduction of the detailed chemistry of the reactions based on experimental data derived through Pressurized Thermogravimetric Balance analysis. The reactions have been effectively modelled in Aspen plus having good information on the gas concentrations along the reactor length.

Author Contributions: Aspen calculations W.L., H.Y. balances correction, Conceptualization, A.A. and F.F.; methodology, M.Z. and A.B.; software, A.C., M.d.L.O.L. and P.B. paper writing and conceptualization. All authors have read and agreed to the published version of the manuscript.

Funding: This work has been partially funded by the GTCLC-NEG project that has received funding from the European Union's Horizon 2020 research and innovation program under the Marie Sklodowska-Curie grant agreement No. 101018756.

Data Availability Statement: Data are publicly available in the project repository in Zenodo: https://zenodo.org/deposit?page=1&size=20 (accessed on 3 April 2023).

Acknowledgments: This work has been funded by the GTCLC-NEG project that has received funding from the European Union's Horizon 2020 research and innovation program under the Marie Sklodowska-Curie grant agreement No. 101018756. Special acknowledgments are given to William A. Rogers of the National Energy Technology Laboratory (US) for helping with the concluding remarks on the arrangements needed to carefully model the effect of the pressure on the PCLC plant.

Conflicts of Interest: The authors declare no conflict of interest.

References

1. Kang, J.-N.; Wei, Y.-M.; Liu, L.-C.; Wang, J.-W. Observing technology reserves of carbon capture and storage via patent data: Paving the way for carbon neutral. *Technol. Forecast. Soc. Chang.* **2021**, *171*, 120933. [CrossRef]
2. Mi, Z.; Meng, J.; Guan, D.; Shan, Y.; Song, M.; Wei, Y.-M.; Liu, Z.; Hubacek, K. Chinese CO_2 emission flows have reversed since the global financial crisis. *Nat. Commun.* **2017**, *8*, 1712. [CrossRef] [PubMed]
3. Black, R.; Cullen, K.; Fay, B.; Hale, T.; Lang, J.; Mahmood, S.; Smith, S. Taking Stock: A Global Assessment of Net Zero Targets. 2021. Available online: https://www.google.com.hk/url?sa=t&rct=j&q=&esrc=s&source=web&cd=&ved=2ahUKEwis1dW5zdD-AhUlmFYBHdzRAe4QFnoECA0QAQ&url=https%3A%2F%2Fca1-eci.edcdn.com%2Freports%2FECIU-Oxford_Taking_Stock.pdf&usg=AOvVaw1ZhRcYFX86SGMCS1CayncH (accessed on 3 April 2023).
4. Vergragt, P.J.; Markusson, N.; Karlsson, H. Carbon capture and storage, bio-energy with carbon capture and storage, and the escape from the fossil-fuel lock-in. *Glob. Environ. Change* **2011**, *21*, 282–292. [CrossRef]
5. Gasser, T.; Guivarch, C.; Tachiiri, K.; Jones, C.D.; Ciais, P. Negative emissions physically needed to keep global warming below 2 °C. *Nat. Commun.* **2015**, *6*, 7958. [CrossRef] [PubMed]
6. Gough, C.; Upham, P. Biomass energy with carbon capture and storage (BECCS or Bio-CCS). *Greenh. Gases Sci. Technol.* **2011**, *1*, 324–334. [CrossRef]
7. Rueda, O.; Mogollón, J.M.; Tukker, A.; Scherer, L. Negative-emissions technology portfolios to meet the 1.5 °C target. *Glob. Environ. Change* **2021**, *67*, 102238. [CrossRef]
8. *Greenhouse Gas Removal*; Royal Society and Royal Academy of Engineering: London, UK, 2019; ISBN 978-1-78252-349-9.
9. Smith, P. Soil carbon sequestration and biochar as negative emission technologies. *Glob. Change Biol.* **2016**, *22*, 1315–1324. [CrossRef] [PubMed]
10. Griscom, B.; Adams, J.; Ellis, P.; Houghton, R.; Lomax, G.; Miteva, D.; Schlesinger, W.; Shoch, D.; Smith, P.; Woodbury, P. Natural climate solutions. *Earth Atmos. Planet. Sci.* **2017**, *114*, 11645–11650. [CrossRef]
11. Smith, P.; Davis, S.J.; Creutzig, F.; Fuss, S.; Minx, J.; Gabrielle, B.; Kato, E.; Jackson, R.B.; Cowie, A.; Kriegler, E. Biophysical and economic limits to negative CO_2 emissions. *Nat. Clim. Change* **2016**, *6*, 42–50. [CrossRef]
12. Fuss, S.; Lamb, W.F.; Callaghan, M.W.; Hilaire, J.; Creutzig, F.; Amann, T.; Beringer, T.; de Oliveira Garcia, W.; Hartmann, J.; Khanna, T. Negative emissions—Part 2: Costs, potentials and side effects. *Environ. Res. Lett.* **2018**, *13*, 063002. [CrossRef]
13. Woolf, D.; Amonette, J.; Street-Perrott, F.; Lehmann, J.; Joseph, S. Sustainable Biochar to Mitigate Global Climate Change. *Nat. Commun.* **2010**, *1*, 56. [CrossRef] [PubMed]
14. Bhave, A.; Taylor, R.H.; Fennell, P.; Livingston, W.R.; Shah, N.; Mac Dowell, N.; Dennis, J.; Kraft, M.; Pourkashanian, M.; Insa, M. Screening and techno-economic assessment of biomass-based power generation with CCS technologies to meet 2050 CO_2 targets. *Appl. Energy* **2017**, *190*, 481–489. [CrossRef]
15. *Climate Intervention: Carbon Dioxide Removal and Reliable Sequestration*; Committee on Geo engineering Climate: Technical Evaluation and Discussion of Impacts; The National Academies Press: Washington, DC, USA, 2015.

16. Harrison, D.P. A method for estimating the cost to sequester carbon dioxide by delivering iron to the ocean. *Int. J. Glob. Warm.* **2013**, *5*, 231–254. [CrossRef]
17. McLaren, D. A comparative global assessment of potential negative emissions technologies. *Process Saf. Environ. Prot.* **2012**, *90*, 489–500. [CrossRef]
18. Sanna, A.; Uibu, M.; Caramanna, G.; Kuusik, R.; Maroto-Valer, M. A review of mineral carbonation technologies to sequester CO_2. *Chem. Soc. Rev.* **2014**, *43*, 8049–8080. [CrossRef]
19. González, M.F.; Ilyina, T. Impacts of artificial ocean alkalinization on the carbon cycle and climate in Earth system simulations. *Geophys. Res. Lett.* **2016**, *43*, 6493–6502. [CrossRef]
20. Renforth, P.; Jenkins, B.; Kruger, T. Engineering challenges of ocean liming. *Energy* **2013**, *60*, 442–452. [CrossRef]
21. Chan, G.G.; Koch, C.M.; Connors, L.H. Blood proteomic profiling in inherited (ATTRm) and acquired (ATTRwt) forms of transthyretin-associated cardiac amyloidosis. *J. Proteome Res.* **2017**, *16*, 1659–1668. [CrossRef]
22. Keith, D.W.; Holmes, G.; Angelo, D.S.; Heidel, K. A process for capturing CO_2 from the atmosphere. *Joule* **2018**, *2*, 1573–1594. [CrossRef]
23. Ghouleh, Z.; Guthrie, R.I.; Shao, Y. Production of carbonate aggregates using steel slag and carbon dioxide for carbon-negative concrete. *J. CO2 Util.* **2017**, *18*, 125–138. [CrossRef]
24. Huijgen, W.J.; Comans, R.N.; Witkamp, G.-J. Cost evaluation of CO_2 sequestration by aqueous mineral carbonation. *Energy Convers. Manag.* **2007**, *48*, 1923–1935. [CrossRef]
25. Möllersten, K. Assessment of classes of CDR methods: Technology Readiness, Costs, Impacts and Practical Limitations of Biochar as Soil Additive and BECCS. *Energy* **2022**, *2004*, 2965.
26. Araújo, O.d.Q.F.; de Medeiros, J.L. Carbon capture and storage technologies: Present scenario and drivers of innovation. *Curr. Opin. Chem. Eng.* **2017**, *17*, 22–34. [CrossRef]
27. Di Giuliano, A.; Capone, S.; Anatone, M.; Gallucci, K. Chemical Looping Combustion and Gasification: A Review and a Focus on European Research Projects. *Ind. Eng. Chem. Res.* **2022**, *61*, 14403–14432. [CrossRef]
28. Kearns, D.; Liu, H.; Consoli, C. *Technology Readiness and Costs of CCS*; Global CCS Institute: Docklands, Australia, 2021.
29. Bartocci, P.; Abad, A.; Bischi, A.; Wang, L.; Cabello, A.; de Las Obras Loscertales, M.; Zampilli, M.; Yang, H.; Fantozzi, F. Dimensioning Air Reactor and Fuel Reactor of a Pressurized Chemical Looping Combustor to Be Coupled to a Gas Turbine: Part 1, the Air Reactor. *Energies* **2023**, *16*, 2102. [CrossRef]
30. Bischi, A.; Langørgen, Ø.; Saanum, I.; Bakken, J.; Seljeskog, M.; Bysveen, M.; Morin, J.-X.; Bolland, O. Design study of a 150 kWth double loop circulating fluidized bed reactor system for chemical looping combustion with focus on industrial applicability and pressurization. *Int. J. Greenh. Gas Control* **2011**, *5*, 467–474. [CrossRef]
31. Bartocci, P.; Abad, A.; Mattisson, T.; Cabello, A.; de las Obras Loscertales, M.; Negredo, T.M.; Zampilli, M.; Taiana, A.; Serra, A.; Arauzo, I. Bioenergy with Carbon Capture and Storage (BECCS) developed by coupling a Pressurised Chemical Looping combustor with a turbo expander: How to optimize plant efficiency. *Renew. Sustain. Energy Rev.* **2022**, *169*, 112851. [CrossRef]
32. Nikoo, M.B.; Mahinpey, N. Simulation of biomass gasification in fluidized bed reactor using ASPEN PLUS. *Biomass Bioenergy* **2008**, *32*, 1245–1254. [CrossRef]
33. Abdelouahed, L.; Authier, O.; Mauviel, G.; Corriou, J.-P.; Verdier, G.; Dufour, A. Detailed modeling of biomass gasification in dual fluidized bed reactors under Aspen Plus. *Energy Fuels* **2012**, *26*, 3840–3855. [CrossRef]
34. Kaushal, P.; Tyagi, R. Advanced simulation of biomass gasification in a fluidized bed reactor using ASPEN PLUS. *Renew. Energy* **2017**, *101*, 629–636. [CrossRef]
35. Puig-Gamero, M.; Pio, D.; Tarelho, L.; Sánchez, P.; Sanchez-Silva, L. Simulation of biomass gasification in bubbling fluidized bed reactor using aspen plus®. *Energy Convers. Manag.* **2021**, *235*, 113981. [CrossRef]
36. Sotudeh-Gharebaagh, R.; Legros, R.; Chaouki, J.; Paris, J. Simulation of circulating fluidized bed reactors using ASPEN PLUS. *Fuel* **1998**, *77*, 327–337. [CrossRef]
37. Cho, P.; Mattisson, T.; Lyngfelt, A. Comparison of iron-, nickel-, copper- and manganese-based oxygen carriers for chemical-looping combustion. *Fuel* **2004**, *83*, 1215–1225. [CrossRef]
38. Abad, A.; García-Labiano, F.; de Diego, L.F.; Gayán, P.; Adánez, J. Reduction Kinetics of Cu-, Ni-, and Fe-Based Oxygen Carriers Using Syngas (CO + H2) for Chemical-Looping Combustion. *Energy Fuels* **2007**, *21*, 1843–1853. [CrossRef]
39. Schuhmann, R. *Technical Publication 1189*; American Institute of Mining and Metallurgical Engineers: New York, NY, USA, 1940.
40. Abad, A.; Adánez, J.; García-Labiano, F.; de Diego, L.F.; Gayán, P.; Celaya, J. Mapping of the range of operational conditions for Cu-, Fe-, and Ni-based oxygen carriers in chemical-looping combustion. *Chem. Eng. Sci.* **2007**, *62*, 533–549. [CrossRef]
41. Ergun, S. Fluid flow through packed columns. *Chem. Eng. Prog.* **1952**, *48*, 89–94.
42. George, S. Entrainment of particles from aggregative fluidized beds. *AIChE Symp. Ser.* **1978**, *74*, 67–74.
43. Tasirin, S.; Geldart, D. Entrainment of FCC from fluidized beds—A new correlation for the elutriation rate constants Ki∞. *Powder Technol.* **1998**, *95*, 240–247. [CrossRef]